/CDFR/PHYS/EXOTICS/CDF-8497
Version 4: February 6, 2007

Run 2 CHAMP search

Thomas Phillips
Duke University

F.D. Snider
Fermilab

February 6, 2007

Abstract

We perform a model-independent search for massive long-lived charged particles using 1.03 fb^{-1} of Run II data collected with the high-p_{t} CMUP trigger. The search uses the Time-of-Flight and COT detectors to isolate slowly-moving, high-p_{t} particles. We observe one candidate event with mass above 100 GeV/c^2 with an expected background of about 1.5 events. Interpreting this result within the context of a reference model with a stable scalar stop squark, we set an upper bound on the production cross section that translates to a lower limit on the mass of 250 at 95% CL. The same result implies a cross section limit of 10 fb at 95% for a weakly-interacting charged stable particle produced with transverse momentum greater than 40 GeV/c, a velocity $0.4 < \beta < 0.9$ within $|\eta| < 1.0$.

Contents

1 Introduction

Extensions to the Standard Model all imply the existence of as yet undiscovered massive particles. In many models, these particles are expected to decay promptly. Most searches consequently attempt to isolate distinctive decay signatures involving leptons, jets and missing transverse energy. Under a variety of circumstances, however, such as a new symmetry, kinematic constraint, weak coupling or barrier in the decay potential, one or more of these new massive particles can acquire a lifetime that is long compared to the typical time required to traverse the detector. In this case, searches based upon a decay signature will fail. If such a particle is charged, it will nonetheless present a very distinctive signature in a detector — that of a slowly moving, high transverse momentum ($p_{\rm t}$) charged track. Attendant with the low velocity is a long time-of-flight (TOF) and an anomalously large ionization energy loss (dE/dx). For a sufficiently massive particle, ionization will dominate the energy loss, even if the particle is strongly interacting [1]. A charged, massive stable particle, or CHAMP, will therefore be highly penetrating and will typically be reconstructed as a muon.

The conditions that lead to the existence of CHAMPs occur in numerous models [2]–[5]. One such example is that of a supersymmetric (SUSY) model with one compactified extra dimension [2]. This model provides a highly specific prediction, that of a stable stop squark with a mass around 200 GeV/c^2. CHAMPs can also arise within the context of SUSY models with gauge mediated SUSY breaking [3]. In these models, the next-to-lightest SUSY partner (NLSP) can become stable if the scale of the SUSY breaking sector is sufficiently large. The stau and stop are considered likely candidates for the NLSP due to electroweak breaking effects. Another model with CHAMPs is that of a fourth generation quark in which the fourth generation is weakly coupled to the other generations [4]. If this coupling is sufficiently small, then one of the heavy quarks can become stable on experimental time scales.

Non-accelerator experiments have ruled out the existence of CHAMPs that have a mass below about 230 GeV/c^2 and that are stable on the time scale of the age of the oceans [6]. The same data excludes CHAMPS with a mass less than about 1 TeV/c^2 and with a lifetime on the scale of the age of the universe, although the limit depends critically on certain details of the thermal history of the universe. In Run 1, CDF placed lower limits of 190 GeV/c^2 on a stable down-like, and 220 GeV/c^2 on a stable up-like fourth generation quark, based upon a search for highly ionizing high-$p_{\rm t}$ particles in the CTC [7]. The ALEPH experiment has also used dE/dx to set a lower limit of 95 GeV/c^2 on a stable stop squark [8]. Stable sleptons have been excluded below a mass of about 99.5 GeV/c^2 based upon the combined results from the LEP2 experiments [9].

A previous CDF preliminary result from Run II based upon a TOF analysis of 53 pb^{-1} found a limit of 107 GeV/c^2 at 95% CL for a stable stop squark[10]. A more recent preliminary result from D0 has set a limit in the range 140–170 GeV/c^2 for a stable chargino based upon an analysis of 390 pb^{-1}. The D0 analysis used muon scintillator detectors to measure the TOF of CHAMP candidate tracks [11].

In this note, we will describe a search for massive stable charged particles conducted by measuring the time-of-flight of high-p_t tracks in 1.03 fb^{-1} collected using high-p_t muon triggers. The present measurement employs a new technique that combines timing information from the TOF and COT detectors, thereby greatly reducing the background relative to that observed using either detector alone. The result of the search will be completely model independent, and can easily be interpreted within the context of a wide variety of models. We choose to quantify the result in terms of a reference stable stop model since the strong production mechanism provides sufficient sensitivity for a significant measurement.

The rest of this note is organized as follows. We first describe the response of the detector to particles with small values of $\beta\gamma$, as expected for CHAMPS. Next, we explain how data from the TOF detector is used to measure the time-of-flight of high-p_t tracks and identify potential CHAMPS. The preparation of the data sample and the estimation of the background rate are discussed in the next two sections, followed by the results of the counting experiment. In the last two sections, we estimate the detection efficiency and present the results in terms of a stable stop model.

2 Datasets and event selection

We search for CHAMPs in high-p_t muon data collected with the CMUP18 trigger and reconstructed by 5.3.1 (the `bhmu0d` dataset) and 6.1.3 production (the `bhmu0h` and `bhmu0i` datasets). This trigger requires XFT tracks and matching muon stubs at L1, and a reconstructed CMUP muon at L3 with $p_t > 18$ GeV/c. We consider all CMUP+CMX+CEM/no-silicon good runs between 141544 and 222524, ignoring CMX run quality for runs before 150145, as defined by the V13 good-run list from the DQM group[12]. The runs must also be included on the CEM good-run list, since we use high-p_t electron data to estimate various detection efficiencies, and therefore need electron and muon samples with identical luminosity weighting..

To reduce the rate of fake muon triggers, a good reconstructed CMUP muon is required in CMUP18 trigger events. The muon ID conforms to the Joint Physics group recommendations circa January, 2007, except that the calorimeter energy requirements are excluded from the selection. The p_t requirement is imposed after applying curvature corrections as described in [13].

Cosmic rays represent a potentially serious background to the analysis since cosmic rays are uncorrelated in time with the event t_0.We remove cosmics from the dataset using the COT di-cosmic tagger[14], where we define a cosmic tag as a track for which the best fit is consistent with either a downward or upward moving cosmic ray with a fit $\chi^2 < 1000$. We remove events in which a reconstructed muon of the trigger type with $p_t > 10$ GeV/c is tagged as a cosmic.

The event selection requirements are summarized in Table 1.

Table 1: Muon dataset requirements. Reconstructed muons must satisfy the Joint Physics high-p_t muon criteria, circa January, 2007, except that calorimeter energy requirements are ignored.

Dataset	Requirements
CMUP	MUON_CMUP18 or MUON_CMUP18_L2_PT15 trigger
	Reconstructed CMUP muon with corrected $p_t > 20$ GeV/c
	No muon with $p_t > 10$ GeV/c that is tagged as a cosmic ray GeV/c

2.1 Datasets for time measurement studies

High-p_t electron events will be depleted in CHAMP candidates, yet qualitatively resemble high-p_t muon events. Electron W and Z events can therefore be used for studies of detector and algorithm performance, reconstruction efficiencies and background studies. The following datasets are used as control samples for these purposes:

- The *Ztight* electron dataset, consisting of tightly selected $Z \rightarrow e^+e^-$ events. This dataset is used in studies of the TOF resolution and in background studies for the analysis.
- The *Wtight* electron dataset, consisting of tightly selected $W \rightarrow e\nu$ events. This dataset is used in studies of the event t_0 reconstruction and in background studies for the analysis. It is also used to determine the selection efficiency for some of the analysis cuts.

3 Detector response to slow particles

While we expect CHAMPS to be penetrating, we must still address the question of whether they would be properly reconstructed by our detector. There are two places where one might expect to find detector inefficiencies for slowly-moving particles: in the tracking of a CHAMP through the COT, and in triggering and reconstructing a CHAMP as a muon. In addition to these potential inefficiencies, the timing measurements in the COT could be biased as a result of the finite road width used in the track reconstruction. We will now discuss all of these potential concerns. (The content in this section is largely reproduced from Ref. [10].)

3.1 Low β Tracking efficiency

For a given drift distance, hits in the COT produced by a slowly moving particle will arrive later than those produced by a particle traveling at c. The pattern recognition, which corrects hit positions under the assumption that they are travelling at c, will fail to find hits and lose track finding efficiency for particles with sufficiently low values of β. To measure this effect, we select a sample of deuterons using a p_t-dependent cut on the dE/dx measured in the COT. Figure 1a

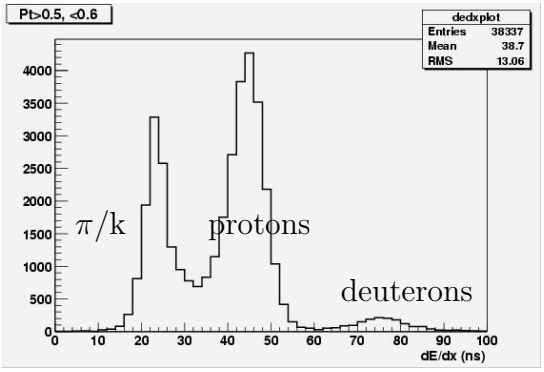

Figure 1: dE/dx for tracks with 0.5 GeV/c < p_t < 0.6GeV/c. Units are in ns, corresponding to the width of the hit read out from the COT. Three regions corresponding to pions/kaons, protons, and deuterons are clearly visible. For a p_t of 0.5 (0.6) GeV/c we select deuterons by requiring that the dE/dx be greater than 73 (67) ns.

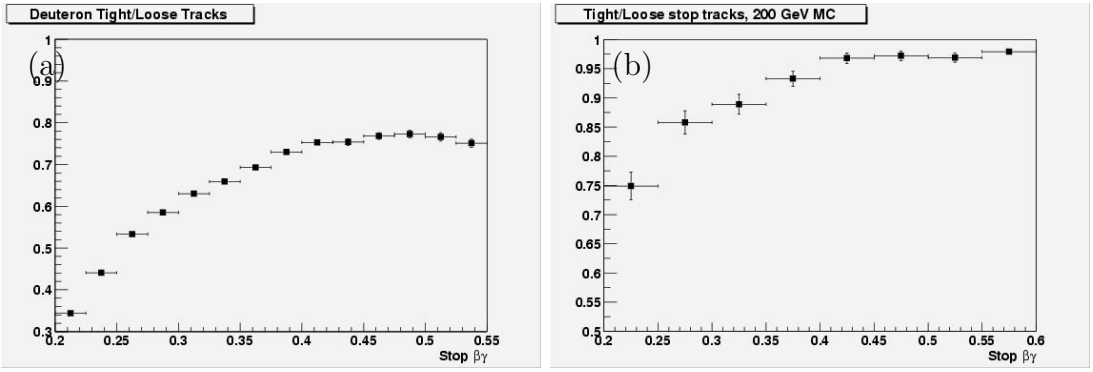

Figure 2: (a) Ratio of tightly to loosely selected tracks which have been identified as deuterons with the dE/dx. (b) Ratio of tightly to loosely selected MC stop tracks. The tracking efficiency is flat for $\beta\gamma > 0.4$.

shows the dE/dx for one slice of the p_t, 0.5GeV/c < p_t < 0.6GeV/c. We apply loose and tight track selection criteria to this sample. The loose selection simply takes all tracks from the default reconstruction, while the tight selection requires more than 25 axial and stereo hits in the COT. We then plot the ratio of loosely and tightly selected tracks as a function of p_t (Figure 2a). The same quantity for tracks from stable stop squarks in Monte Carlo events is shown in Fig. 2b. In both of these studies, the ratio is flat for $\beta\gamma$ greater than 0.4. We conclude that the tracking efficiency is constant for $\beta\gamma > 0.4$.

For this analysis, we will demand that all candidate tracks have a p_t such that β is greater than 0.4 in order to insure that there is no loss of tracking efficiency due to low β effects. This requirement implies a cut of approximately $p_t > 80\,\mathrm{GeV}/c$ for a CHAMP mass of 200 GeV/c^2, and $p_t > 40\,\mathrm{GeV}/c$ for a

CHAMP mass of 100 GeV/c^2.

3.2 Muon trigger and reconstruction

Muons are reconstructed by associating a track found in the COT with a stub found in the muon chambers. The default muon reconstruction requires that a stub in the CMU (CMP) be within 10 (20) cm of the track extrapolation. For this analysis, we use the much tighter muon identification criteria defined by the Joint Physics group. The reconstruction extrapolates the track assuming that the underlying particle was travelling at c. In Ref. [10], we determine that the timing windows within the muon detectors and reconstruction are is sufficiently wide that this assumption does not introduce an inefficiency for reconstructing a slowly-moving CHAMP in the CMUP.

Using a trigger simulation, the same study determined that the CMUP trigger is fully efficient for any CHAMP that can be tracked through the COT. The situation for the CMX trigger, however, is different since the CMX trigger includes a scintillator requirement. The timing gates placed around the expected arrival time for prompt muons may sculpt the CHAMP acceptance. We have not fully evaluated the impact of this effect on the CMX trigger efficiency for CHAMP events, and have therefore elected to exclude the CMX dataset from the current analysis.

4 Time-of-flight measurements

The TOF detector consists of 216 scintillator bars arranged in a cylinder around the COT. Each bar is about 280 cm long and about 4 cm on a side. Photomultiplier tubes (PMT's) are mounted on the east and west side of each bar and are read out by ADMEM's (to get pulse height information) and TDC's (to get timing information). The design timing resolution is about 100 ps for a hit that is recorded by both PMT's. A more detailed description of the detector can be found in Ref. [15].

We define the time-of-flight for a particle by the expression

$$TOF = t_a - t_0 \tag{1}$$

where t_a is the arrival time of the particle at the inner surface of the first TOF bar hit, and t_0 is the interaction time for the event. We take arrival times from the standard 6.1.4 TOF reconstruction[16]. This algorithm extrapolates tracks to the TOF and discriminates good track–TOF matches based upon requiring consistency between the times and pulse heights measured from the two ends of the bar. The matching criterion, based upon a match chi-squared, is optimized to minimize the likelihood of large measurement errors caused by multiple particles – many of which are not found as tracks – hitting the bar. In a later section, we investigate how changes to the matching chi-squared requirement change the sensitivity of the analysis.

The arrival times are corrected for channel-to-channel differences, propagation delay in the TOF bars and slewing effects that result from the fixed threshold discriminators used to generate the timing signals. The slewing corrections are particularly important since they vary over a range of more than 1 ns, well in excess of the design time resolution of 100 ps. Small but significant velocity dependent corrections are not applied to the CHAMP candidates. These effects typically introduce errors no larger than a few hundred pico-seconds.

After calculating the arrival time for all tracks, we calculate an independent estimate of the event t_0 with a sub-set of tracks that originate from the primary event vertex, excluding the track for which we want a velocity measurement. For the present analysis, we also exclude any track with $p_{\rm t} > 20$ GeV/c in order to avoid contamination of the t_0 calculation from potential signal tracks or other high-$p_{\rm t}$ tracks used as a control sample. (The motivation for the 20 GeV/c requirement is discussed in Sect. 6.1. We use the t_0 fitter from the standard reconstruction to estimate the event t_0 from the specified sub-set of tracks. The fitter simultaneously takes into account all possible particle hypotheses weighted according to the particle ID from dE/dx when available, or assuming 80% pions, 10% kaons and 10% protons when it is not.

Once the event t_0 is determined, we estimate the time-of-flight of high-$p_{\rm t}$ CHAMP candidates using Eq. 1. We then calculate the β of the particles from the time-of-flight and the path-length of the track trajectory from the vertex to the TOF detector. Finally, we combine the β and track momentum (p) measurements to estimate the "TOF mass" ($m_{\rm TOF}$) of the candidates:

$$m_{\rm TOF} = p\sqrt{\frac{1}{\beta^2} - 1} \tag{2}$$

The TOF mass can be used to further reduce background, as will be discussed later.

In the rest of this section, we will discuss the performance of the TOF timing measurements and the t_a and t_0 time resolution functions.

4.1 Measurement of arrival time for high-$p_{\rm t}$ tracks

High-$p_{\rm t}$ tracks used in this analysis must either be identified as good muons or as high-quality tracks. The track selection used in both cases conforms to the selection required for high-$p_{\rm t}$ lepton identification, and includes the following:

- $p_{\rm t} > 20$ GeV/c.
- At least 3 axial super-layers with ≥ 5 hits.
- At least 2 stereo super-layers with ≥ 5 hits.
- $|d_0| < 0.05$ cm for silicon tracks, 0.5 cm for COT-only tracks.
- z_0 within 5σ of a class 12 or better vertex.
- $|z_0| < 60$ cm.
- TOF match chi-squared < 14 (the standard requirement).

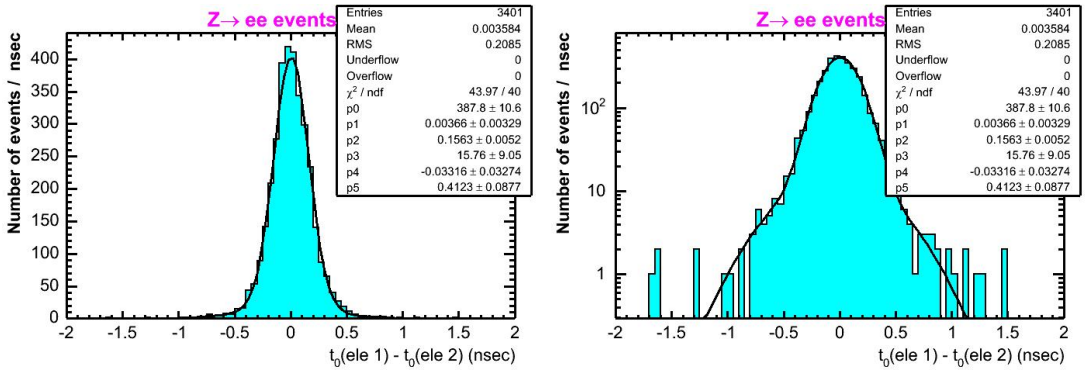

Figure 3: Production time difference between Z electrons as measured by TOF detector.

To study the arrival time error function, we use the two electron tracks in $Z \to e^+e^-$ events with tight selection criteria. We can estimate the production times of each electron leg. These times should both equal the event t_0. The distribution of production time differences, $\Delta(t_p) = t_0(\text{ele 1}) - t_0(\text{ele 2})$, is $sqrt2$ times the symmetrized time resolution function. In Fig. 3, we show the $\Delta(t_p)$ distribution for all Z events. The central core of the distribution is approximately Gaussian with a width of 156±5 ps, corresponding to an arrival time resolution of 110 ps. A second Gaussian fit to the tails of the distribution has a width of 410±90 ps.

A total of 13 of 6802 tracks, or 1.9%, have an error that is larger than 1 ns. Without additional background suppression, this error rate will be the limiting factor on the sensitivity of the analysis.

Figures 4 and 5 show the distribution of estimated $\Delta(t_p)$ measurement uncertainties, $\sigma(t_p)$, and normalized production time differences, $\Delta(t_p)/\sigma(t_p)$. The central portion of the latter plot has a width near unity, indicating that the measurement uncertainties accurately reflect the errors for the core of the time resolution function.

4.2 Event t_0 measurement

To find the event t_0, we use the standard t_0 fitter from the 6.3.4 TOF reconstruction [16] plus some minor improvements. The changes are documented in Ref. [17], and have been blessed by the B-group for inclusion in the next release of the reconstruction. Tracks used in the t_0 calculation are selected as part of the analysis. As noted previouly, we remove all potential CHAMP candidate tracks from the sample of tracks used to determine the event t_0 by requiring $p_{\rm t} < 20$ GeV/c. In addition to these cuts, we require the following:

- Track z_0 within 5σ of the class 12 vertex with maximum sum-$p_{\rm t}$
- $|d_0| < 1.5$ cm for both SVX and COT tracks

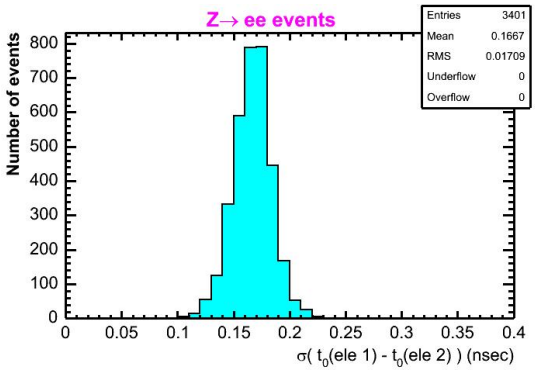

Figure 4: Uncertainty in the production time difference for the two Z electron legs.

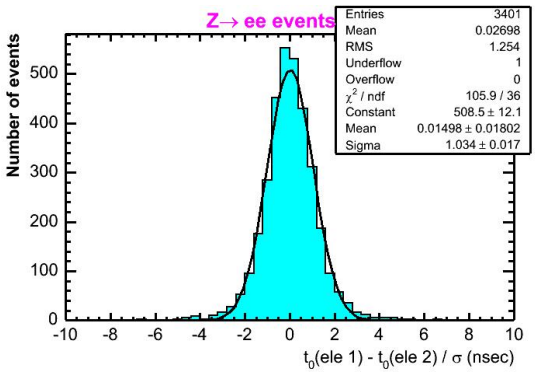

Figure 5: Production time difference between Z electron legs normalized by the uncertainty.

- TOF match $\chi^2 < 14$ (the standard cut)

No additional hit requirements are imposed beyond those required for the track to be included in `defTracks`.

We study the performance of the t_0 fitter in tight $W \to e\nu$ events. Figure 6 shows the t_0 distribution for all electron W events. While the distribution for a single run is approximately Gaussian, changes in mean t_0 over time produce the skewed shape observed. (Note that the TOF calibration does not constrain the mean t_0 to any particular value.)

The t_0 time resolution is a strong function of the number of tracks used in the t_0 fit. To measure the time resolution function, we first split the tracks available for the t_0 calculation in each event into two sub-sets with an equal number of tracks in each. The splitting algorithm alternates down a p_t ordered list so that both sub-sets have a representative range of track momentum. We then fit the t_0 for each sub-set and compare the difference, $\Delta(t_0)$. The resulting distribution is shown in Fig. 7. To obtain the t_0 resolution, we fit the distribution to a double Gaussian. We take the width of the narrow core to be the resolution.

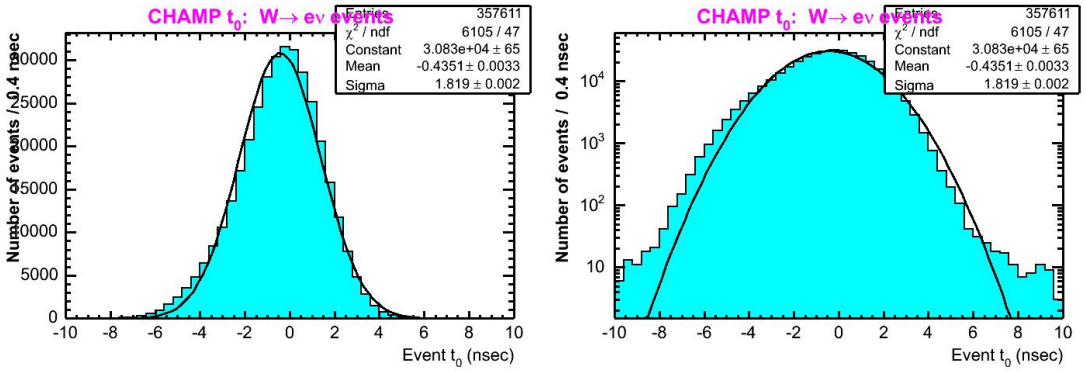

Figure 6: TOF t_0 distribution for electron W events.

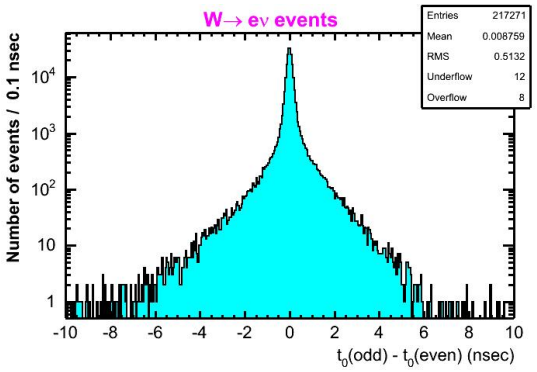

Figure 7: Distribution of $\Delta(t_0)$, the difference between the t_0 determined using one half of the tracks in the event with that found using the other half.

In Fig. 8, we show the t_0 resolution as a function of the number of tracks in the t_0 calculation. The asymptotic value is about 50 ps. Figure 9 shows the distribution of the number of tracks available for the t_0 calculation in electron W events. This distribution should be comparable to that found in CHAMP events.

A more important consideration for the CHAMP analysis is the fraction of events with large t_0 errors. Fig. 10 shows the fraction of events in which $\Delta(t_0)$ exceeds some specified value, plotted as a function of the number of tracks used in the t_0 fit. At the average t_0 multiplicity of about four tracks, approximately 1% of events have a t_0 error that is about 1 ns or larger. With seven or more tracks, the error rate is a few per mille or less.

4.3 Velocity measurements

Given the arrival times and the event t_0 we can calculate the TOF for tracks. Figure 11 shows the difference between the TOF measured for electrons in the tight $W \rightarrow e\nu$ sample and that expected for a particle travelling at c. The

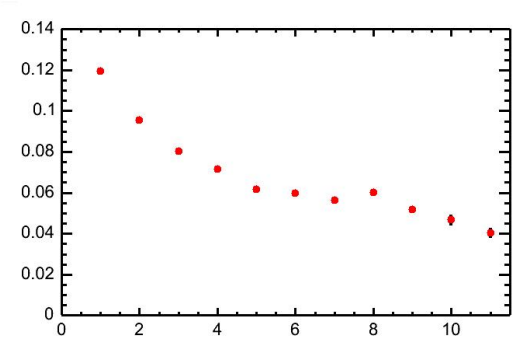

Figure 8: Resolution of the TOF event t_0 as a function of the number of tracks available for the fit.

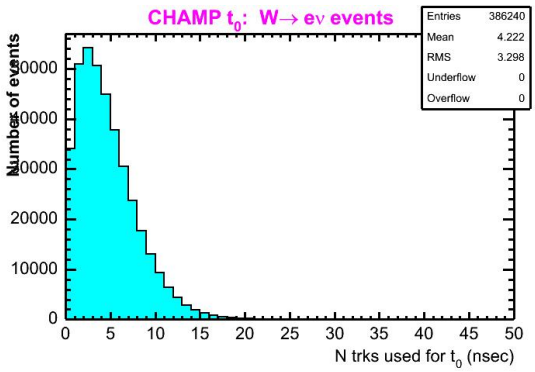

Figure 9: Number of tracks available for t_0 calculation in electron W events. Only tracks with $p_{\rm t} < 20$ GeV/c are considered.

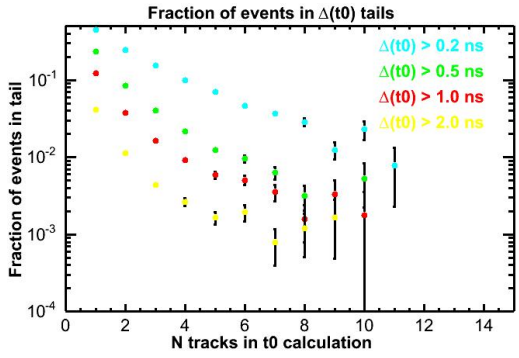

Figure 10: Fraction of events in which $\Delta(t_0)$, the difference between the t_0 estimated by two equal-sized sub-sets of tracks, differs by more than the specified time, measured as a function of the number of tracks used in the t_0 fit. This function measures the rate at which the t_0 fit incurs a large non-Gaussian error.

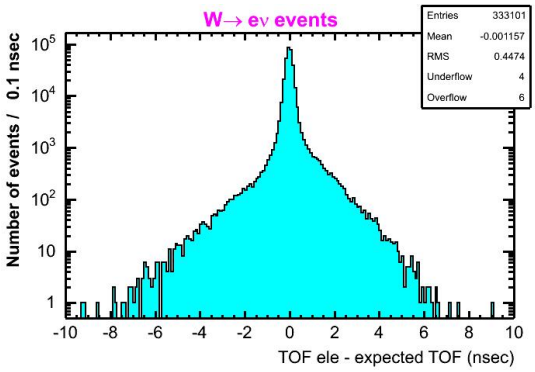

Figure 11: Difference between the TOF for W electrons and that expected for a particle moving at c.

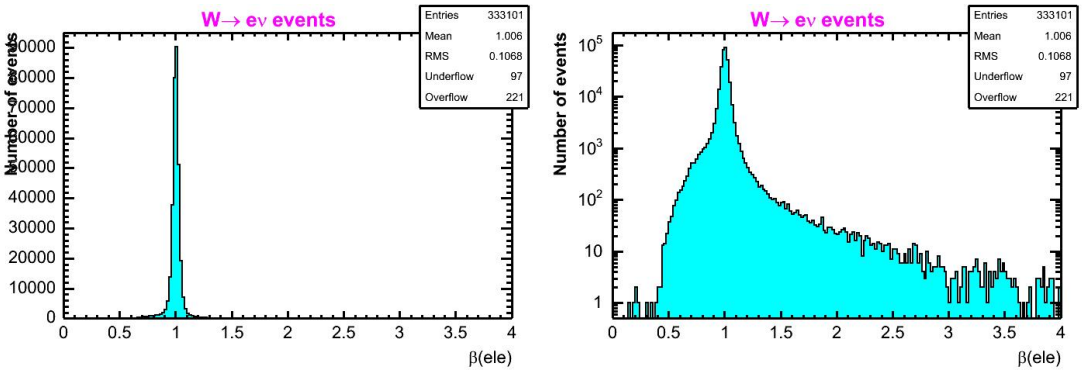

Figure 12: The β for W electrons measured by the TOF detector.

tail on the right side of the plot include measurements with errors that mimic slower moving particles, and contributes to the instrumental background in the CHAMP search. The tail on the left side of the plot represents and inefficiency, but not a source of background.

From the track TOF and the extrapolation of the track to the TOF detector, we calculate the velocity of the particle. Figure 12 shows the β distribution for electrons in the tight W sample. In this plot, we see a long tail at large β that can be ignored, except for the effect on the signal detection efficiency. The low side tail in this case will contribute to the background. Since we know the true velocity of the electrons, we can calculate the pull distribution for the electron beta measurement, which is shown in Fig. 13

5 COT timing measurements

The COT has 96 measurement layers, each of which provides an independent timing measurement that include, among other things, the drift time for the

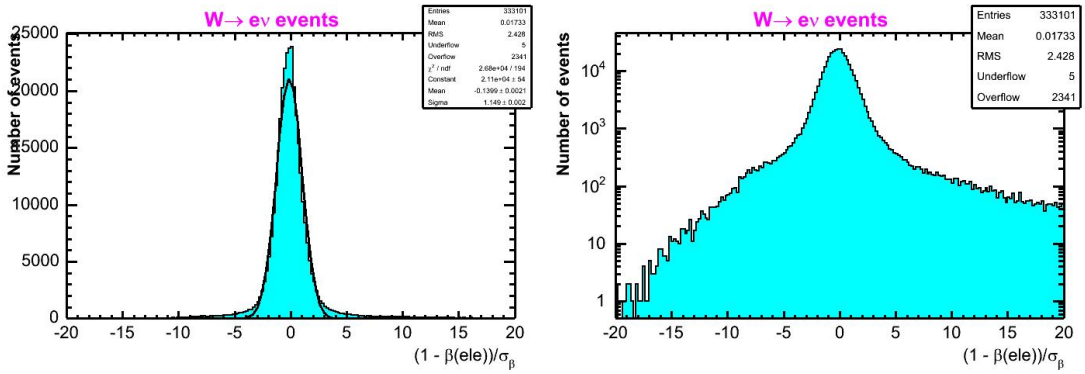

Figure 13: The pull distribution for β measured by the TOF for W electrons.

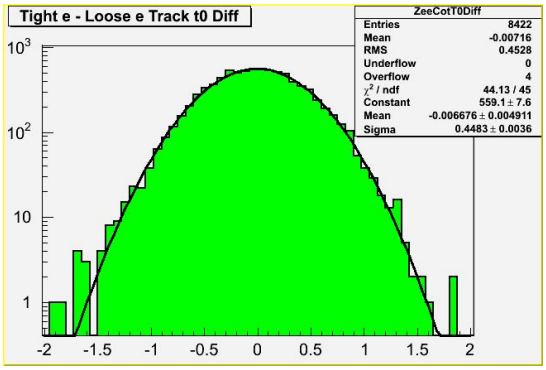

Figure 14: Difference in the production times measured by the COT for the two electron legs in $Z \rightarrow e^+e^-$ events.

ionization to reach the wire plus a the arrival time of the track at the wire. By comparing nearby hits that have opposite drift directions, one can estimate the common arrival time component. Unless this component is correctly subtracted, these hits will have an apparent offset relative to a (locally) straight track trajectory. The arrival time time component also includes two contributions, one from the production time of the track and another for the time-of-flight for the particle from the production vertex to the wire. These simple observations underlie the algorithm used to extract production time and velocity information from the COT.

The details of this algorithm are documented in [18]. Here we will briefly describe how the algorithm is used to estimate the production time of the track. Assuming that the particle velocity is known and that there is an equal number of hits with each drift sign, then the average signed residual (the residual multiplied by the drift direction) to the track fit will be the drift distance corresponding to the production time for the track.

To find the event interaction time, we use the class `Cot_tZero`. This class

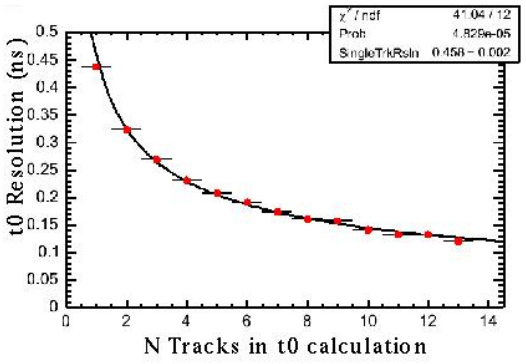

Figure 15: Event COT t_0 resolution as a function of the number of tracks used in the calculation.

calculates the event t_0 from an arbitrary collection of tracks in two passes. The first pass finds the t_0 for each track by essentially averaging the signed residuals using a wide road for hit selection and assuming the particle is traveling at the speed of light. A measure of how well the t_0 measurement works for individual tracks is shown in Fig. 14, which compares the COT track t_0 for the two electrons from Z decays. Note that while the width of this distribution is signficantly larger than that of the corresponding distribution for TOF arrival time measurements, the COT measurements lack the large non-Gaussian tails observed in the TOF measurements.

The track t_0's are next averaged to find a preliminary interaction t_0. In the second pass, tracks are assumed to have a production time equal to this preliminary t_0. A tighter hit-selection road is then used to re-calculate t_0 values for each track assuming a particle velocity as calculated from the measured momentum and each of three mass hypotheses (proton, kaon and pion). The best event t_0 is then calculated with the same algorithm as that used for the TOF event t_0, except that dE/dx information is not used to re-weight the mass hypotheses.

As is the case for tracks used in the TOF event t_0, all tracks used in the COT event t_0 calculation must have $p_{\rm t} < 20$ GeV/c and a beamline-corrected z_0 within 5σ of the class 12 or better vertex with the maximum sum-$p_{\rm t}$. Figure 8 shows the COT event t_0 resolution as a function of the number of tracks in the fit. The average number of tracks in the t_0 fit is about 9.3 (Fig. 16), compared to about 4.2 (Fig. 9) in the TOF t_0 fit.

In order to compare the COT t_0 to the TOF t_0, it is necessary to calibrate the systems relative to each other since they do not use the same definition for time zero. We have done this for all runs with good muons and good TOF information.

Beyond directly comparing TOF and COT t_0 values, a second way we use the COT is to calculate χ^2 values for different velocity and t_0 hypotheses. For example, we can assume the event t_0 and track velocity as measured by the TOF system and refit COT track. A large fit χ^2 indicates an inconsistency between

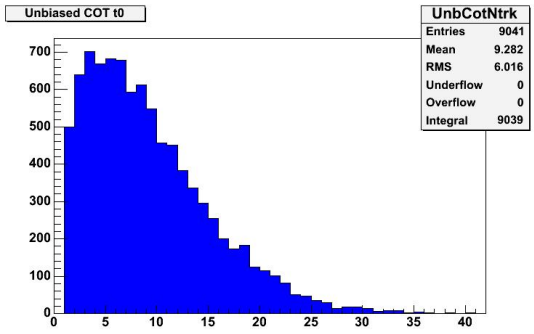

Figure 16: Number of tracks in COT t_0 calculation for electron W events.

the TOF and COT timing measurements, and can be used to identify and reject tracks or events with significant mis-measurements in the TOF.

We note here that the COT is capable of identifying CHAMPs on its own without using the TOF system. While the resolution with the COT is not as good as that with the TOF system (compare Figs. 15 and 8), the COT timing resolution function is nearly Gaussian, which leads to highly a predictable instrumental background. In addition, the higher efficiency in the COT contributes to increased acceptance for candidate tracks and higher multiplicities in the event t_0. Pursuing such a search will be the topic of a future note.

6 Event reconstruction and analysis

To proceed with the analysis and background estimation procedure, we must first classify the tracks and events we find in the various data samples. The purpose of this exercise is to reduce the background in the signal sample and isolate a background-enriched sample in which to estimate the background,

6.1 Track classification

CHAMPs produced at CDF will typically have very high transverse momentum. Figure 17 shows the distribution of reconstructed $p_{\rm t}$ in MC data for stable stops with masses of 100 GeV/c^2 (solid blue) and 200 GeV/c^2 (dashed red). As a first step in reducing background, we require that a CHAMP candidate tracks have $p_{\rm t} > 40$ GeV/c and have a good TOF match as defined in Sect. 4.1. In addition, it must either be identified as a good muon as described in Sect. 2 or as a good track according to the track quality cuts for high-$p_{\rm t}$ lepton identification:

- $p_{\rm t} > 20$ GeV/c.
- $p < 420$ GeV/c.
- At least 3 axial super-layers with ≥ 5 hits.
- At least 2 stereo super-layers with ≥ 5 hits.

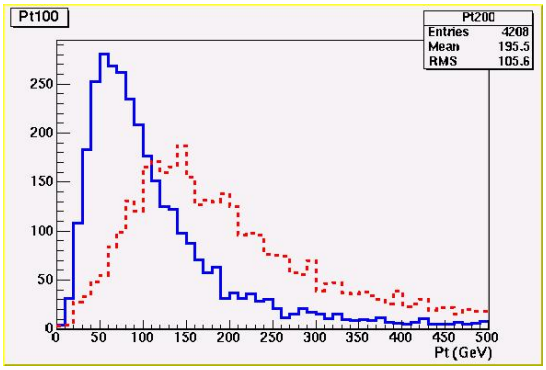

Figure 17: Reconstructed p_t distribution for stable stop squarks with a mass of 100 GeV/c^2 (solid blue histogram) and 200 GeV/c^2 (dashed red histogram).

- $|d_0| < 0.02$ cm for silicon tracks, 0.2 cm for COT-only tracks.
- z_0 within 5σ of a class 12 or better vertex.
- $|z_0| < 60$ cm.

In all cases, the measured p_t includes curvature corrections [13]; tracks without silicon hits are first beam-constrained[1]. Tracks satisfying these criteria are classified as *signal region* or *candidate* muons and tracks. We allow a maximum of two candidate tracks per event. If more than two tracks pass these criteria, only the two highest-p_t are considered as *candidate* tracks.

Tracks with corrected p_t in the range $20 < p_t < 40$ GeV/c will be depleted in CHAMP signal (for CHAMP masses greater than 100 GeV/c^2) relative to signal region tracks and are used to predict the background within the signal region. To be considered for this purpose, the track must either be identified as a good muon using the Joint Physics muon identification but excluding the calorimeter energy requirements, or be identified as a good track using the same criteria outlined for signal region tracks. The second track or muon must be associated with the same vertex as the trigger muon. We define these tracks as *control region* tracks. Again, we allow at most two control region tracks per event, and consider only the two highest-p_t tracks in the event of more.

All tracks with $p_t < 20$ GeV/c that have COT hits and are associated with the event vertex are classified as *COT t_0 tracks* and are used to calculate the COT event t_0. COT t_0 tracks that also have TOF measurements are classified as *TOF t_0 tracks* are are used in the TOF event t_0 calculation.

6.2 Event classification

The analysis extracts two disjoint sub-samples of events from the high-p_t muon dataset. An event is considered to be in the *signal sample* if it has at least one

[1] This prescription for the measured p_t conforms to that specified by the Joint Physics Group for high-p_t lepton identification, and will be used for all high-p_t momentum measurements in this analysis.

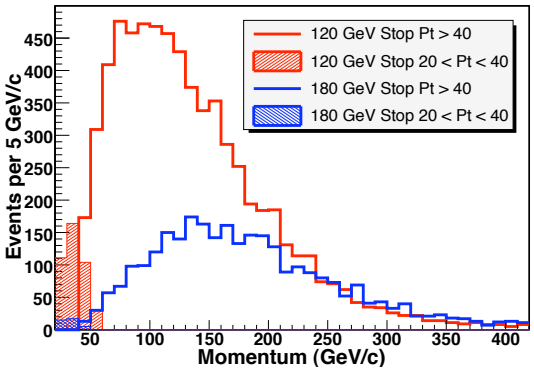

Figure 18: Reconstructed momentum for 120 GeV stop (red) and 180 GeV stop (blue). The shaded histograms are events in the control region.

signal region muon. A second signal region muon or non-muon signal region track will also be considered as a candidate track and will enter the analysis. Control region tracks within signal events do not enter the analysis in any way.

An event belongs to the *control sample* if it does not belong to the signal sample and has at least one control region muon. A second control region muon or non-muon control region track will also enter the analysis as a control region track.

6.3 Post-production event reconstruction

We re-process a portion of the 5.3.1 and 6.1.3 production output in order to improve the use of timing information in the data. First, we run the ZVertexFinder from 6.3.4 in order to gain the vertexing efficiency and background rejection in the 5.3.1 production data [19].

Next, we re-run the TOF reconstruction in order to include the changes discussed in Ref. [17] and Sect. 4.2, and to select the tracks to include in the TOF t_0 calculation. For both the TOF and COT t_0 calculation, we define the event vertex as the beamline-corrected z_0 of the leading signal region track in candidate events, or the leading control region track in control events. All TOF t_0 tracks with beamline-corrected z_0 within 5σ of this event vertex used in the TOF t_0 calculations if the corrected p_t is less than 20 GeV/c.

To further reduce background, we exploit the expected correlation between the CHAMP velocity and momentum and look for a signal in the distribution of TOF mass, $m_{\rm TOF}$, from Eq. 2. Figure 18 shows the expected momentum for our reference model of a stable stop for masses of 120 GeV/c^2 and 180 GeV/c^2; Figure 19 shows the TOF mass distributions for masses of 140 GeV/$c^2$and 200 GeV/c^2. To calculate $m_{\rm TOF}$, we use the track momentum following the Joint Physics Group convention. For comparison, we show the reconstructed momentum, TOF β and TOF mass for electron tracks in the tight $W \rightarrow e\nu$ sample in Figs. 20–22, respectively.

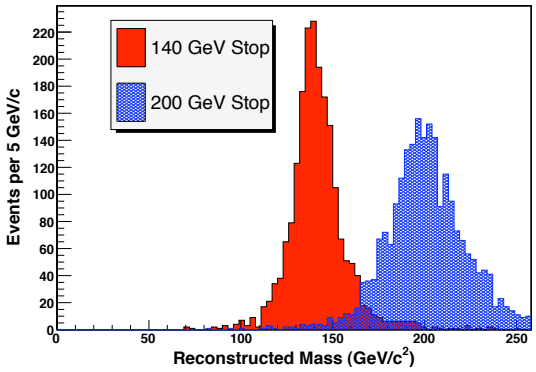

Figure 19: Reconstructed mass for 140 GeV stop (red) and 200 GeV stop (blue).

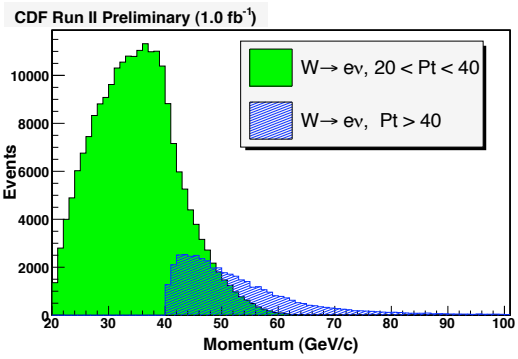

Figure 20: Momentum for the control region and signal region in the $W \rightarrow e\nu$ dataset.

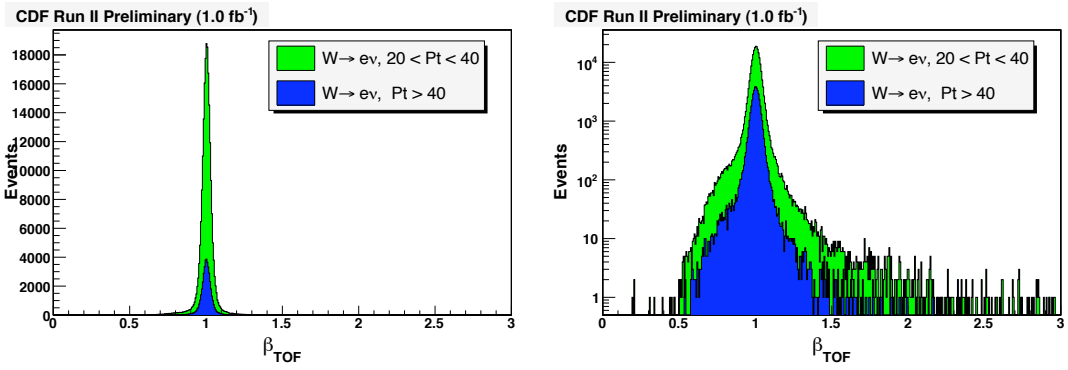

Figure 21: W electron β distribution as measured by the TOF detector.

Next, we use the algorithms described in Sect. 5 to to calculate the t_0 for each track with COT hits, the COT event t_0 and, for high-p_t tracks, the χ^2 of the COT track fit assuming the value of β as measured by the TOF. The

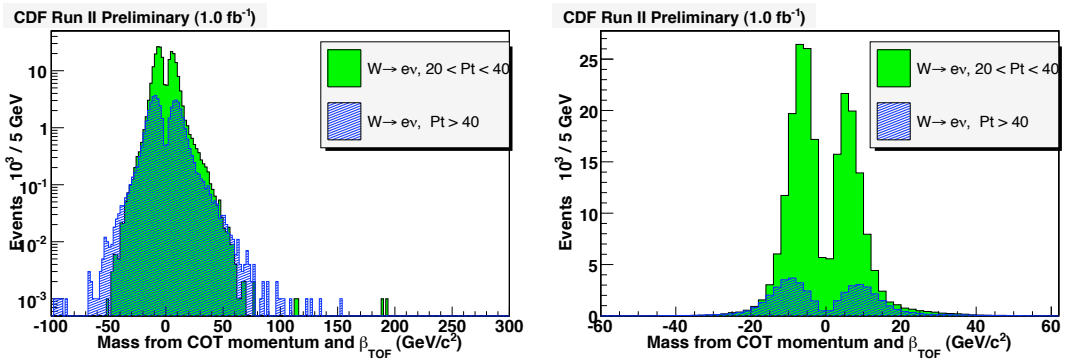

Figure 22: TOF mass distribution for W electrons within the control (green) and signal (blue) regions.

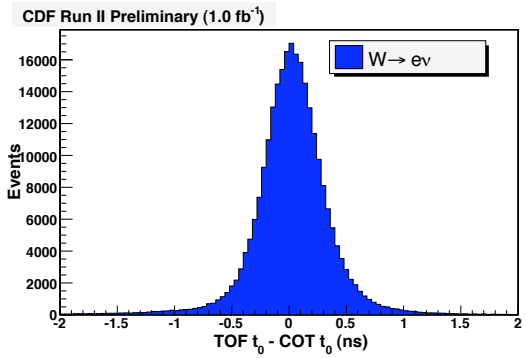

Figure 23: Distribution of time difference between t_0 values estimated using the COT and TOF detectors.

latter two quantities allow us to quantify the consistency between COT and TOF timing measurements and are useful in reducing background in the TOF measurements (described in the next section). Figures 23 and 24 show the event-by-event difference between the TOF and COT event t_0 values and the COT fit χ^2 assuming the TOF β value, respectively, for W electrons.

6.4 Analysis procedure

All timing information for signal region muons has been blinded during the development of the analysis techniques, background reduction and estimation. The electron W and Z samples are used to study the performance of the time measurements and cross-check the background estimation procedure. The background reduction techniques were developed and optimized using the predicted background in the W electron sample in order to avoid tuning based on fluctuations in the signal dataset. The *a priori* optimization criterion in all cases was to min-

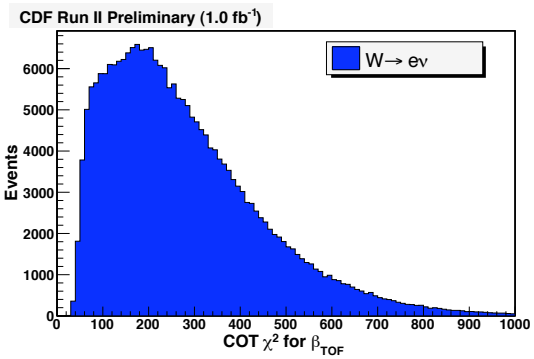

Figure 24: χ^2 for COT fit assuming $\beta_{\rm TOF}$ in the $W \to e\nu$ dataset.

imize the expected cross section limit assuming the background in a luminosity-weighted electron W sample. For this calculation, we assume the background in the W sample is the same as that in the muon sample, and use the acceptance for the reference stable stop model to evaluate the cross section limit. We also calculate the probability of discovery assuming the stable stop model in case the optimum differs for the two. In practice, the low background and relatively high efficiency of the major analysis cuts rendered a formal optimization step unnecessary.

We also decided *a priori* how to treat a significant excess over background (i.e., greater than 3σ) should one be observed. The first step is to use additional information from the detector to confirm the probability of having observed slow particles. The additional handles available include timing data from the EM and hadron calorimeters and muon detectors, and pulse height data from the COT, TOF and calorimeters. A real CHAMP event would likely produce anomalous signals in several of these detectors, which would strengthen any observation using time-of-flight alone.

7 Background Estimates

Since there are no Standard-Model CHAMPs, the only background we expect comes from cosmic rays that trigger the detector and introduce tracks uncorrelated in time with any interaction events, and from instrumental effects. We reduce the potential background from cosmic rays, which are uncorrelated with the interaction time, by rejecting events with tagged cosmic muons as described in Sect. 2. We reduce the potential background from cosmic rays by rejecting events with tagged cosmic muons as described in Sect. 2. Using TOF information alone, instrumental effects produce a large background of fake CHAMP candidates [10]. In the present analysis, we eliminate the bulk of this background by comparing timing information from the TOF with that from the COT within each event, and by conducting the search within the $m_{\rm TOF}$ distribution.

In the following sections, we discuss the details of the background suppression

and estimation methods.

7.1 Instrumental background

Timing errors from instrumental effects fall into three categories:

1. mis-measured interaction times (t_0);
2. mis-measured candidate arrival times (t_a); and
3. mis-measured momenta.

A large momentum mis-measurement can lead to a high TOF mass even if the velocity is near $\beta = 1$. In general terms, we reduce the background from timing errors by requiring consistency between the TOF and COT measurements. Background from large momentum errors can be reduced by requiring the measured β to differ significantly from unity. We then predict the shape of the remaining background in the signal region by using information from tracks in the control region, as will be described below.

7.1.1 Instrumental background suppression

In order to understand and reduce the high-mass CHAMP background, we use well-identified high-$p_{\rm t}$ electrons in $W \to e\nu$ events. We do not expect to find any real CHAMPs in this sample, so all the electron candidates are assumed to be traveling with $\beta = 1$. In Fig. 25, we show the measured TOF mass distribution for electron tracks after applying several sets of background reduction criteria. The top histogram (green) shows the TOF mass distribution for all electron tracks (both signal-region and control-region) in the $W \to e\nu$ dataset. Here, we observe a significant number of events in the mass region above 100 GeV/c^2. The second histogram (blue) shows the effect of requiring that the TOF t_0 be no more than 0.5 ns earlier than the t_0 calculated from COT tracks. This requirement has some effect on the high-mass tail, but primarily removes events in the 25-100 GeV/c^2 mass range.

The third histogram (red) in Fig. 25 results after requiring the measured velocity to be significantly different from c, specifically $\beta_{\rm TOF} < 0.9$. This cut removes some tracks in the high-mass tail and of course all negative-mass events, which correspond to cases where we measure $\beta_{\rm TOF} > 1$. Most of the remaining events are some combination of mis-measured TOF arrival times for the candidate track and residual events with mis-measured t_0's. We identify and remove some of these events by requiring a COT track fit $\chi^2 < 500$ when $\beta_{\rm TOF}$ is assumed in the fit. In the electron dataset, this criterion removes all but one of the remaining events with TOF mass above 100 GeV/c^2. The resulting mass distribution is shown in cyan in Figure 25.

7.1.2 Instrumental background estimation procedure

In order to predict the shape of the mass distribution, we make the assumption that the velocity measurement errors are uncorrelated with the track momentum.

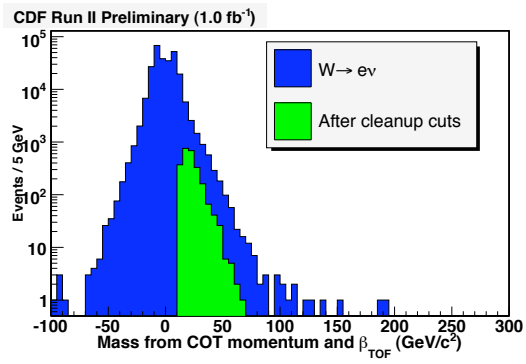

Figure 25: Mass calculated from $\beta_{\rm TOF}$ and the track momentum for the $W \rightarrow e\nu$ dataset. The blue histogram is all events; the green is after applying background supression cuts.

For the signal these quantities are correlated by the mass of the CHAMP (see Equation 2). This assumption allows us to predict the background in the signal region by convolving the β distribution measured using control region tracks with the momentum distribution of tracks within the signal region. The control region tracks will be dominated by muons from W and Z boson decays and other SM sources, plus fake muons and muons from decays-in-flight. In all cases, the muons are known to be travelling at c. The general tracking environment for these muons will be very similar to that found in the higher-$p_{\rm t}$ muons of the signal region as well, making the control region muons an ideal sample with which to perform this calculation.

To check the assumption that the velocity measurement errors are independent of the momentum, we first convolve the TOF β distribution for control region electrons in tight electron W events with the momentum distribution for these same tracks to make a prediction for the mass distribution in the control region. The left plot in Figure 26 shows the prediction (red curve) superimposed upon the measured mass distribution (histogram). The integral plot is shown to the right. None of the background suppression criteria in Sect. 7.1.1 have been applied to this sample, but they have for Figure 27.

We next use the β distribution from control region electrons to predict the background for signal region electrons. Fig. 28 shows the resulting background prediction (red curve) super-imposed on the observed TOF mass distribution for signal region electrons (green histogram) before applying the background suppression criteria. Once we apply the background suppression cuts (Fig. 29, we observe no background for $m_{\rm TOF}$ greater than 80 GeV/c^2. In both cases, we find good agreement with the background prediction.

We conclude that the β measurement errors are indeed independent of the track momentum for high-$p_{\rm t}$ electron tracks, and now turn our attention to background predictions for the muon data.

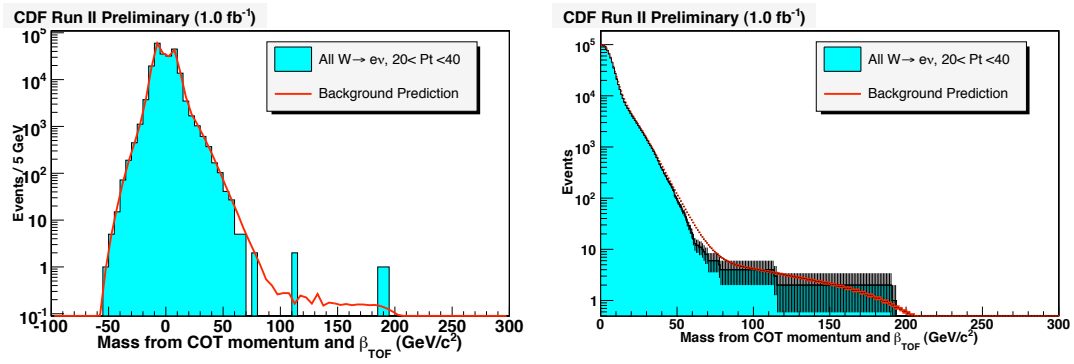

Figure 26: Control-region mass calculated from $\beta_{\rm TOF}$ and the track momentum for the $W \rightarrow e\nu$ dataset. The histogram contains all control-region events, while the red line is the prediction made assuming β and momentum are independent. The plot on the left is the differential histogram; the integral histogram is on the right.

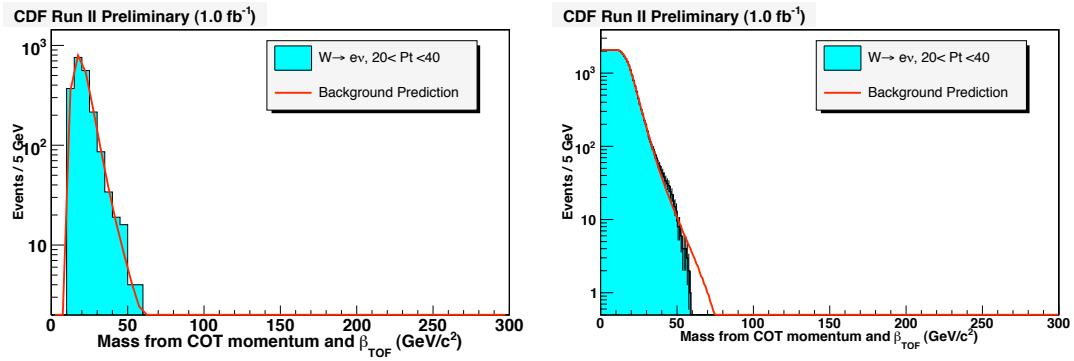

Figure 27: Control-region mass (after cleanup cuts) calculated from $\beta_{\rm TOF}$ and the track momentum for the $W \rightarrow e\nu$ dataset. The histogram is for all control-region events, while the red line is the prediction.

7.1.3 Instrumental background in the muon data

The muon data has some sources of background that are not included in the electron data, such as cosmic rays and muons from decays-in-flight. We will discuss the issue of cosmic rays separately. In order to understand whether decays-in-flight and other differences between the characteristics of electron and muon tracks alter the predictability of the background, we will examine the background predictions and observations within the control sample of the muon dataset.

The first question is whether the background suppression requirements also suffice to suppress background in the muon sample. Fig. 30 shows the mass distribution for control sample CMUP muons with $30 < p_{\rm t} < 40$ GeV/c before and after all background suppression cuts are applied. No events remain at

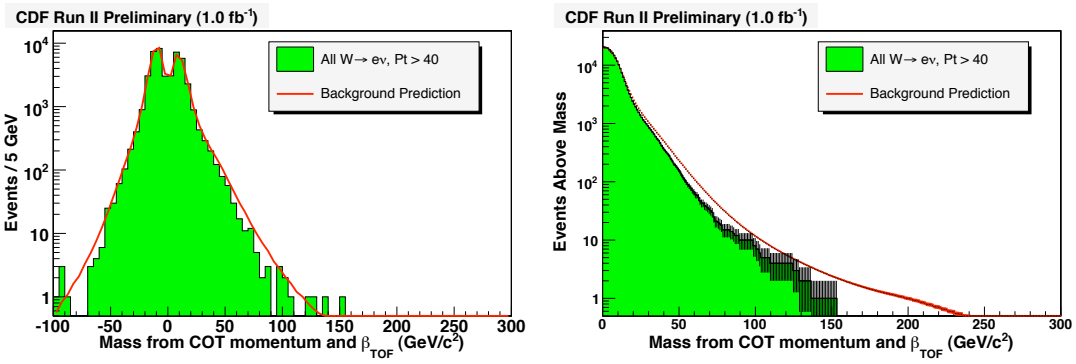

Figure 28: TOF mass distribution for signal-region electron tracks in the $W \rightarrow e\nu$ dataset before excluding backgrounds. The histogram is for all signal-region tracks, while the red line is the prediction using the β distribution for tracks in the control-region. The plot on the left is the differential histogram; the integral histogram is on the right. The shape of the high-mass tail of the prediction is determined by the few events in the control sample with very low measured β and the high-momentum tracks in the signal region.

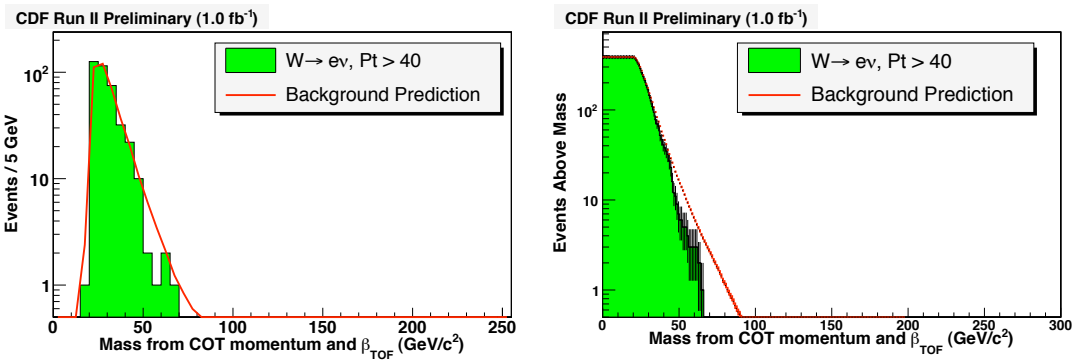

Figure 29: Observed and predicted TOF mass distribution for signal-region W electron tracks after applying background suppression cuts. We use the β distribution of control region electrons to predict the signal region background.

masses above about 80 GeV/c^2 after applying all cuts.

In the same plot, we show the predicted background. To mimic the effect of using the β distribution from a distinct momentum range to model the background, we have used the β distribution for muons with $20 < p_t < 30$ GeV/c and the momentum distribution for tracks for $30 < p_t < 40$ GeV/c to predict the background for muons with $30 < p_t < 40$ GeV/c. We see good agreement between the background predictions and observations, again verifying the basic assumption that the β errors are independent of momentum. Figure 31 shows an expanded view of the observed and predicted background for the high-p_t control

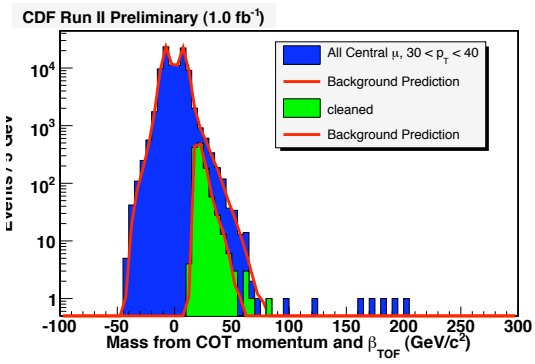

Figure 30: TOF mass distribution for the CMUP control sample. The blue histogram is for all events, while the green histogram is after requiring the COT and TOF t_0's to agree. The red curve is the predicted background based upon the β distribution for tracks with $20 < p_{\rm t} < 30$ GeV/c and the momentum distribution for tracks with $30 < p_{\rm t} < 40$ GeV/c.

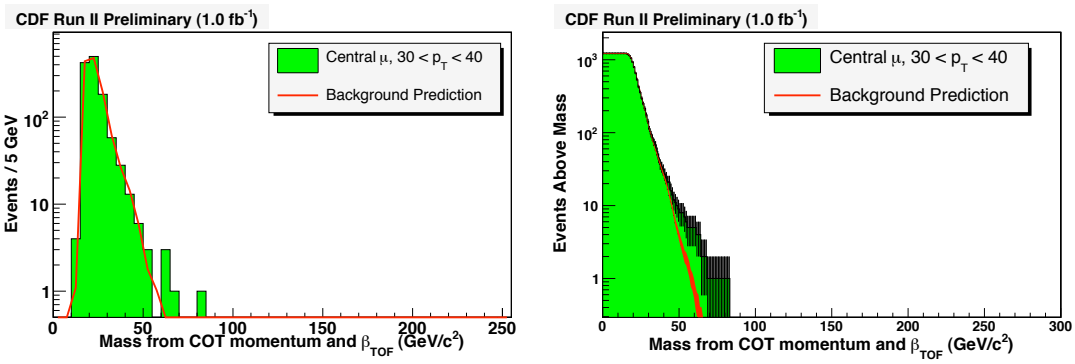

Figure 31: Mass calculated from $\beta_{\rm TOF}$ and the track momentum for the CMUP control dataset. The histogram is for muons with $30 < p_{\rm t} < 40$ GeV/c after background suppression cuts, while the red line is the prediction using the β distribution for control region muons with $20 < p_{\rm t} < 30$ GeV/c.

region CMUP muons after all background suppression.

We will now estimate the background in the signal sample of the muon data using the β distribution from the muon control sample and the momentum distribution from the signal sample. In Figs. 32, we show the integral of the predicted CMUP signal region TOF mass background as a function of the various background suppression requirements. The width of the curves indicate the statistical uncertainty in the predictions. We estimate that for masses above about 150 GeV/c^2 we expect two events or less. after applying all suppression cuts. The statistical uncertainty for the integrated background above about 100 GeV/c^2 is significantly smaller than unity.

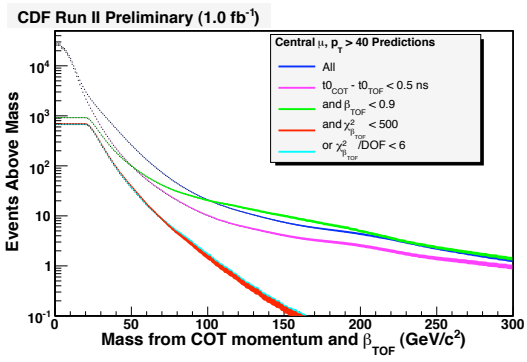

Figure 32: Integral plot of the predicted TOF mass background for signal region CMUP muons as a function of the various background suppression requirements.

7.1.4 Systematic uncertainties

The scale of the systematic uncertainty in the background estimate is determined by the statistical precision with which we have tested how well the estimation procedure models the background. We have not yet preformed a quantitative estimate of this agreement. Qualitatively, the agreement in all control samples appears within statistical uncertainties, although there is some evidence in the signal-region electron data that the prediction over-estimates the high-mass background rate . These observations suggest that the systematic uncertainties are at the same scale as the statistical uncertainties. We will see in Sects. 8 and 9 that the systematic uncertainty in the stop detection efficiency dominates all other uncertainties. We can therefore ignore this uncertainty in the search.

An additional background error is incurred if there are CHAMP candidates in the signal region. In this case, the additional high-p_t tracks from the CHAMPs can add to the predicted high-mass background rate. Since the background prediction is based upon uncorrelated β and momentum values, the additional background will likely be small. We can test this conjecture explicitly by MC distributions to those measured in data, but have not yet performed this test.

7.2 Cosmic rays

Since cosmic rays are uncorrelated in time, it is possible for the arrival times to appear to make a very slow, high-p_t track if compared to the event t_0. To determine the effect of residual cosmic rays in the analysis, we first isolate a tightly identified sample of cosmic rays. Figures 33 and 34 show the correlation between the impact track impact parameter and, respectively, the number of tracks with z_0 within 5σ of the z_0 for the cosmic ray candidate, and the χ^2 from the di-cosmic fit for events tagged as cosmics by our cosmic ray filter. We see residual beam-beam events at small impact parameter, and define a tight cosmic ray sample by excluding the small impact parameter regions in these plots.

We then pass the tightly selected cosmic ray events through the analysis, but

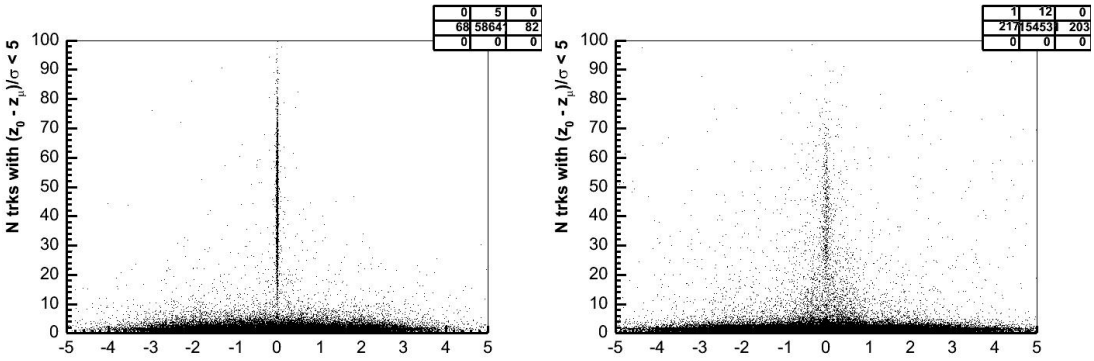

Figure 33: Number of tracks with a z_0 within 5σ of the muon z_0 versus the muon d_0 for SVX and COT tracks for muons removed from the data sample by the cosmic-ray filter.

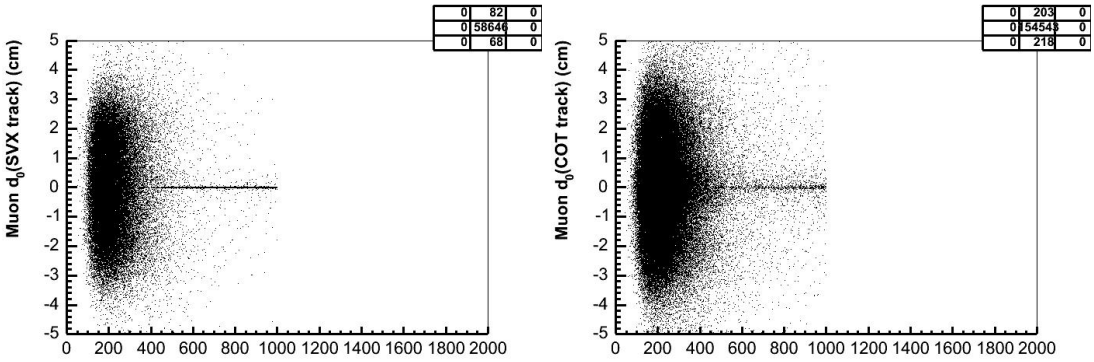

Figure 34: Muon d_0 for SVX and COT tracks versus the chi-squared from the di-cosmic fit for muons removed from the data sample by the cosmic-ray filter.

excluding the impact parameter and cosmic ray cuts. Of approximately 150k events with tagged cosmic ray muons, four pass the event selection and enter the signal region. All of these events are eliminated by the background suppression requirements. Since the number of residual cosmic rays in the muon data after applying cosmic ray removal is significantly smaller than the number of tagged cosmic ray events, we conclude that the residual cosmic ray background in the TOF mass plot is negligible.

8 Results

The observed TOF mass distribution for signal region CMUP muons is shown in Figures 35 and 36. The top histogram (green) shows all the signal-region events before the background suppression cuts. The suppression cuts are applied successively, finally resulting in the bottom histogram (cyan), which contains

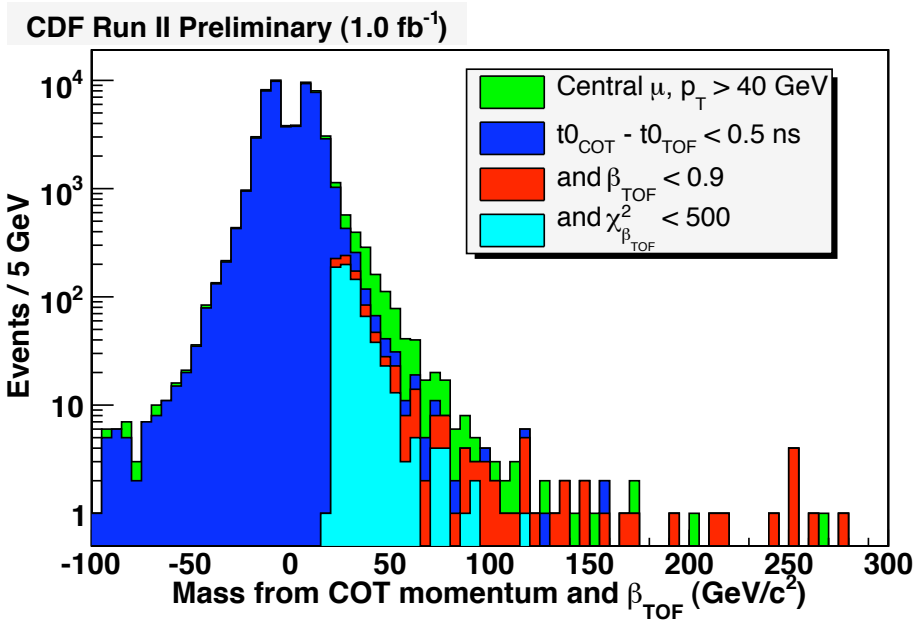

Figure 35: Mass calculated from $\beta_{\rm TOF}$ and the track momentum for candidate tracks in the CMUP dataset. The green histogram is for all events, while the blue histogram is after requiring the COT and TOF t_0's to agree. The red histogram also requires $\beta_{\rm TOF} < 0.9$, and the cyan histogram requires a good COT χ^2 assuming $\beta_{\rm TOF}$.

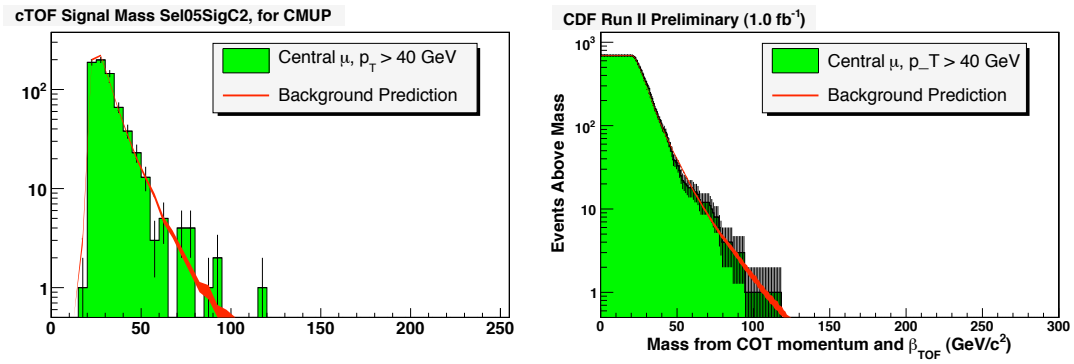

Figure 36: Mass calculated from $\beta_{\rm TOF}$ and the track momentum for the central muon dataset. The histogram is for events after cleanup cuts, while the red line is the prediction using the $20 < p_T < 40$ GeV control-region β.

our signal result. We observe one event with a reconstructed TOF mass above 100 GeV/c^2 and no events with a reconstructed TOF mass above 120 GeV/c^2, the mass range of interest for this search.

We can use these results to set model-independent limits on strongly-interacting and weakly interacting CHAMPs. Model-dependent factors include efficiencies

across kinematic variables such as β and momentum, and geometric acceptance. We can define a model-independent result by specifying the observed limit for CHAMPs that are fiducial to the TOF detector with $P_t > 40$ GeV and $0.4 < \beta < 0.9$. The efficiency for detecting CHAMPs within these ranges can be understood from the data without reference to any CHAMP model. We can then set separate limits for strongly and weakly interacting CHAMPs.

Because we expect CHAMPs to be pair produced, we calculate the efficiencies for one or two fiducial CHAMPs. The case with two fiducial CHAMPs requires special care, because it is possible for one CHAMP to trigger the event but fail the JP muon ID criteria, while the second CHAMP does not cause the trigger but passes the JP muon ID. The efficiency for a single fiducial CHAMP to be in our sample is $\epsilon_{chrg}\epsilon_{JP}\epsilon_{trig}\epsilon_{cosmic}$. Here ϵ_{chrg} is the efficiency for the particle to be charged (unity for a weakly interacting charged particle, close to 0.5 for a strongly interacting particle after hadronization), ϵ_{JP} is the Joint-Physics muon efficiency without the E_{EM} or E_{HAD} cuts, ϵ_{trig} is the muon trigger efficiency, and ϵ_{cosmic} is the efficiency for a non-cosmic track to pass the cosmic veto filter. The efficiency for an event with two CHAMPs fiducial to the CMUP to make it into our analysis is

$$2\epsilon_{chrg}\epsilon_{JP}\epsilon_{trig} - (\epsilon_{chrg}\epsilon_{JP}\epsilon_{trig})^2 + 2(\epsilon_{chrg}(1-\epsilon_{JP})\epsilon_{trig})(\epsilon_{chrg}\epsilon_{JP}(1-\epsilon_{trig}))$$

where for simplicity we have neglected ϵ_{cosmic} which is very close to unity ($0.9982\pm$ 0.0001, measured in $W \rightarrow e\nu$). The first product is the sum of the probabilities for each CHAMP to be accepted, the second product subtracts the double counting when both CHAMPs are accepted, and the third product adds the probability that one CHAMP will trigger but fail the muon selection while the second CHAMP fails the trigger but passes the muon selection. The factor of two in the last product accounts for the fact that there are two ways to do this. The above efficiency simplifies to

$$(\epsilon_{chrg}\epsilon_{JP}\epsilon_{trig})^2 + 2((\epsilon_{chrg}\epsilon_{JP}\epsilon_{trig})(1-\epsilon_{chrg}(1-\epsilon_{JP}-\epsilon_{trig})))$$

For the record, the uncertainty on this is

$$\sqrt{\begin{array}{c}\delta^2_{\epsilon_{chrg}}\Big[2\epsilon_{JP}\epsilon_{trig}\big[1+\epsilon_{chrg}\epsilon_{JP}\epsilon_{trig}-4\epsilon_{chrg}\big(1-\epsilon_{JP}-\epsilon_{trig}\big)\big]\Big]^2 \\ +\delta^2_{\epsilon_{JP}}\Big[2\epsilon_{chrg}\epsilon_{trig}\big[1+\epsilon_{chrg}\big(\epsilon_{JP}(2+\epsilon_{trig})+\epsilon_{trig}-1\big)\big]\Big]^2 \\ +\delta^2_{\epsilon_{trig}}\Big[2\epsilon_{chrg}\epsilon_{JP}\big[1+\epsilon_{chrg}\big(\epsilon_{trig}(2+\epsilon_{JP})+\epsilon_{JP}-1\big)\big]\Big]^2\end{array}}$$

In order for an event with two fiducial CHAMPs to be accepted, we only require a single muon trigger and a single good JP muon in the same detector, but we do not require the two to match. Since the efficiency for a good JP muon to trigger is very high, the correction is small due to one CHAMP passing the trigger but failing the JP selection while the other CHAMP fails the trigger but passes the JP selection. Nevertheless, we have included this contribution to our acceptance.

Requirement	Efficiency	Source
$\|Z_0\| < 60$ cm	0.958 ± 0.002	CDF8318
CHAMPs vertex z match	0.8569 ± 0.0005	$W \to e\nu$
TOF t_0	0.9109 ± 0.0004	$W \to e\nu$
COT —TOF t_0 match	0.9543 ± 0.0004	$W \to e\nu$
Net Efficiency	0.714 ± 0.002	

Table 2: Event-level efficiencies related to the event vertex requirements.

Requirement	CMUP Efficiency	CMX Efficiency
Track COT hits	0.9999 ± 0.0001	0.9997 ± 0.0002
$d0$ cut	0.9852 ± 0.0007	0.9984 ± 0.0007
δx CMU	0.9956 ± 0.0009	—
δx CMP	0.9813 ± 0.0019	—
δx CMX	—	0.9965 ± 0.0011
isolation (sliding)	0.9768 ± 0.0021	0.9807 ± 0.0025
Net Efficiency	0.940 ± 0.003	0.975 ± 0.003

Table 3: Efficiencies related to CMUP and CMX ID requirements. These are luminosity-weighted averages of the efficiencies for the 0d, 0h, and 0i datasets listed in CDF-8618, Table 10

Detection efficiencies are listed in Tables 2–4. All efficiencies have been measured from data, usually the $W \to e\nu$ sample; the sources of the efficiencies are listed in the tables.

The efficiency for associating a track with a vertex, which we find to be 85.7%, has two components: the efficiency for the vertexing algorithm to find the vertex (which is high) and the efficiency for a given track z_0 to be within 5σ of the vertex z. This last efficiency indicates that the reported measurement uncertainties are underestimated, possibly caused by mis-identified silicon hits, but we also believe that some of the tracks failing this cut have badly mismeasured momenta and would make a significant contribution to our high-mass background.

We find that the efficiency for finding a TOF match varies significantly between the electron and the muon datasets, and that it falls significantly during the run, presumably because of the gain loss in the TOF system and because of increased occupancy. We use these variations to set the uncertainties at 3% on the TOF match efficiencies to account for possible model dependence with CHAMPs. We expect CHAMPs fiducial to the CMUP detector to have efficiencies closer to the muons, and we use the electrons from W decay that are not fiducial to the CMUP to estimate the efficiency for CHAMPs that are not fiducial to the CMUP.

The CHAMP detection efficiency is significantly different for weakly and strongly interacting CHAMPs. As is described in considerable detail in CDF6307 [10],

Requirement	Efficiency	Source
TOF fiducial CMUP	0.9870 ± 0.0002	muon dataset
TOF pulse match (CMUP)	0.717 ± 0.03	muon dataset
TOF pulse match (not CMUP)	0.635 ± 0.03	$W \to e\nu$
$\beta_{TOF}\chi^2 < 500$	0.8871 ± 0.0007	$W \to e\nu$
Net TOF Efficiency (CMUP)	0.64 ± 0.04	
Net TOF Efficiency (not CMUP)	0.56 ± 0.05	

Table 4: Efficiencies related to the Time-of-Flight requirements. We find significantly different efficiencies in the electron an muon samples, and the efficiency drops significantly during the run, presumably due to TOF gain losses and increased occupancy due to luminosity. As a result, we use these variations to set the uncertainties on the TOF match efficiencies to account for possible model dependence.

the efficiency for a strongly interacting heavy quark or squark to be charged is $(52.9 \pm 2.3)\%$. In order for the CHAMP to trigger the muon system, the CHAMP must be charged when it traverses both the muon detectors and the tracking chamber. Charge exchange interactions in the calorimeter further reduce the fraction of initially charged, strongly interacting CHAMPS that reach the muon detectors as charged particles. As a result, the net CMUP trigger efficiency is $(39.6 \pm 6.6)\%$.

Using the CMUP trigger efficiency, we estimate an overall detection efficiency for a single fiducial, strongly interacting CHAMP of $(8.8 \pm 1.6)\%$. Given one observed candidate events with $m_{\rm TOF}$ above 100 GeV/c^2 in 1.03 fb^{-1}, we calculate a model-independent limit[2] for strongly interacting CHAMPs *that are fiducial to the TOF system and fall within our kinematic acceptance* of $\sigma < 48$ fb at 95% C.L. Similarly, the acceptance for a weakly interacting CHAMP is $(38 \pm 2)\%$, which leads to a model-independent limit of $\sigma < 10$ fb at 95% C.L. for weakly interacting CHAMPs *that fall within our kinematic and geometric acceptances.*

In the next section, we present the results for a specific model, that of a stable stop squark.

9 Results for a stable stop squark

In Figure 19 we show the reconstructed masses for 120 GeV/c^2 and 180 GeV/c^2 stable stop CHAMP MC data. The stop MC is described in detail in CDF6307 [10]. In this note, we will only describe the efficiencies related to the present analysis.

Because we expect stops to be pair produced, we need to classify events according to where the two tracks go in the detector. As previously described, we require a trigger track in the CMUP.The second stop can be found as a CMUP

[2] We calculate all limits using a Bayesian approach assuming a flat prior with the `bayesianlimit` package [24] posted on the statistics committee web page [23].

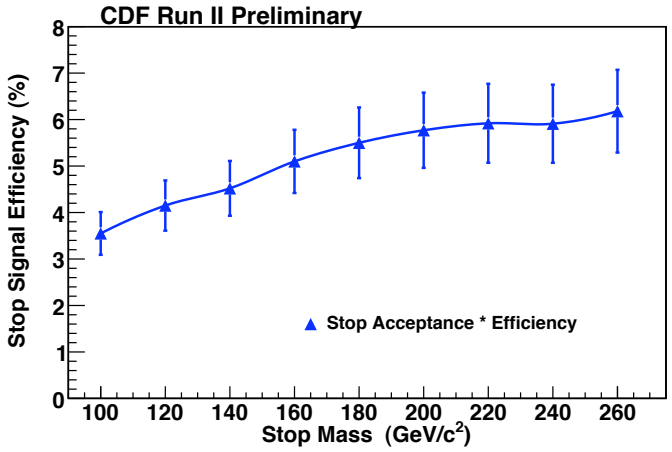

Figure 37: Acceptance times efficiency as a function of stop mass.

muon, a CMX muon, a track or missed entirely. All CMUP tracks are fiducial to the TOF, but only some of the other tracks are.

The efficiency for detecting stop CHAMPs include all the efficiencies described in the previous section for strongly-interacting CHAMPs. The vertex efficiency includes the requirement that the track z_0 be within ± 60 cm, and having a good match between the COT and TOF t_0. The inefficiency is dominated by the 52.9% efficiency that the stop will hadronize as a charged particle (Details of the hadronization calculation can be found in Ref. [10].) It also includes muon ID (including isolation but without EM or hadronic energy cuts) and losses to the cosmic filter. Finally, there is an efficiency for tracks fiducial to the TOF to have good matches to TOF pulses.

Geometric and kinematic acceptances were determined from the Monte Carlo and are dependent upon the stop mass. We use the special version of Pythia modified to properly hadronize the stops that is described in CDF6307 [10], but updated to the version in cdfsoft2 6.1.4mc to get the current detector simulation. Geometric acceptance using the CMUP ranges from 49% for 100 GeV/c^2 stop to 65% for 260 GeV/c^2 stop. Total efficiencies are listed in Table 5 and the net efficiency is plotted as a function of mass in Figure 37. These efficiencies along with the theoretical cross sections give the total number of events expected in 1.03 fb^{-1}, also listed in Table 5 and plotted in Figure 38. For the purpose of counting events for a given mass m, we count all events with $m_{\rm TOF} > 0.8m$, which is 96% – 99% efficient for the masses considered. No upper limit on the mass window is used in order to reduce our sensitivity to our model of the TOF mass line shape. We will impose an upper limit on the mass window if we relax our upper limit on the track momentum. Since our expected background is low and falls with mass, this one-sided mass window only adds a small background to each mass point.

The dominant systematic uncertainties are in the probability for the stop to

Mass (GeV/c^2)	100	120	140	160	180
CMUP CMUP	1.7 %	2.0 %	2.1 %	2.6 %	3.0 %
CMUP + TOF	1.5 %	1.9 %	2.2 %	2.5 %	2.7 %
CMUP only	1.7 %	1.9 %	2.0 %	2.0 %	2.0 %
CHAMP Acc * Eff	4.9 %	5.8 %	6.3 %	7.1 %	7.6 %
Net Reconstructed	$3.5 \pm 0.5\%$	$4.2 \pm 0.5\%$	$4.5 \pm 0.6\%$	$5.1 \pm 0.7\%$	$5.5 \pm 0.8\%$
Cross section (NLO)	14.7	5.3	2.2	1.0	0.48
N Expected 537	227	102	52	27	

Mass (GeV/c^2)	200	220	240	260
CMUP CMUP	3.2 %	3.5 %	3.4 %	3.7 %
CMUP + TOF	2.9 %	2.9 %	3.0 %	3.1 %
CMUP only	1.9 %	2.0 %	1.9 %	1.9 %
CHAMP Acc * Eff	8.0 %	8.2 %	8.2 %	8.6 %
Net Reconstructed	$5.8 \pm 0.8\%$	$5.9 \pm 0.8\%$	$5.9 \pm 0.8\%$	$6.2 \pm 0.9\%$
Cross section (NLO)	0.24	0.13	0.069	0.038
N Expected	14	7.8	4.2	2.4

Table 5: Efficiencies for various stop masses. The first set of numbers include the geometric and kinematic acceptances as well as trigger, TOF, and identification efficiencies for the various detectors where the second CHAMP can go. These are summed to give the CHAMP acceptance times efficiency, which is the efficiency for at least one CHAMP to be identified in our final sample given that it passes the vertex selection. This efficiency is multiplied by the vertex efficiency of $(71.4 \pm 0.2)\%$ to get the Net Efficiency.

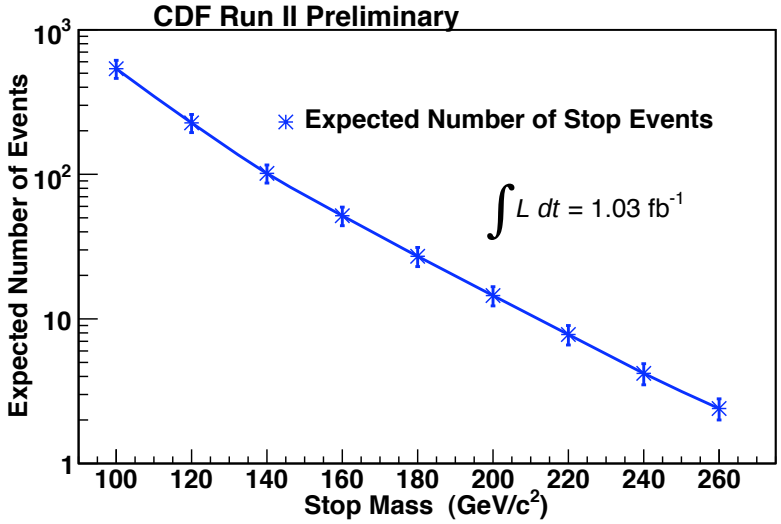

Figure 38: Stop expected signal and background as a function of stop mass.

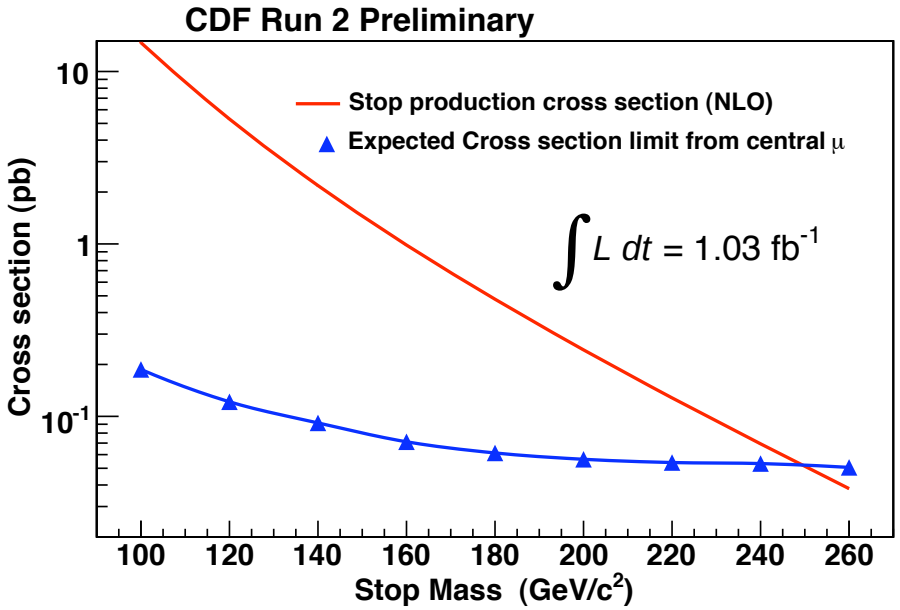

Figure 39: The theoretical NLO cross section for stop production, calculated using the Prospino program[22], is plotted as a function of stop mass (red), along with the limits expected for this analysis given the efficiencies shown in Table 5 and the predicted background. Expected limits are shown for the CMUP only (blue).

hadronize or rehadronize as a charged particle. Systematic uncertainties in the background estimate are small by comparison.

With these acceptances, we are able to use the predicted background shape to determine our expected 95% C.L. upper limits on the stop production cross section. These limits are shown as a function of stop mass in Figure 39, along with the NLO theoretical stop production production cross section calculated with the Prospino2 program [22] and CTEQ5 parton distribution functions.

We observe 1 track with $m_{\rm TOF}$ greater than 100 GeV/c^2 and none above 120 GeV/c^2 in 1.03 fb^{-1} of CMUP data. Assuming the null hypothesis, we calculate the 95% C.L. upper limit on the stop production cross shown in Fig. 40. The limit of about 50 fb at high mass corresponds to a lower limit on the mass of a stable stop of 250 GeV/c^2.

10 Conclusions

We have performed a model independent search for charged, massive stable particles using timing information from the TOF and COT detectors. The search is performed in 1.03 fb^{-1} of data collected with a high-$p_{\rm t}$ CMUP trigger. To conduct the search, we have developed a new technique for identifying large mismeasurements in the TOF system by requiring consistency with COT timing

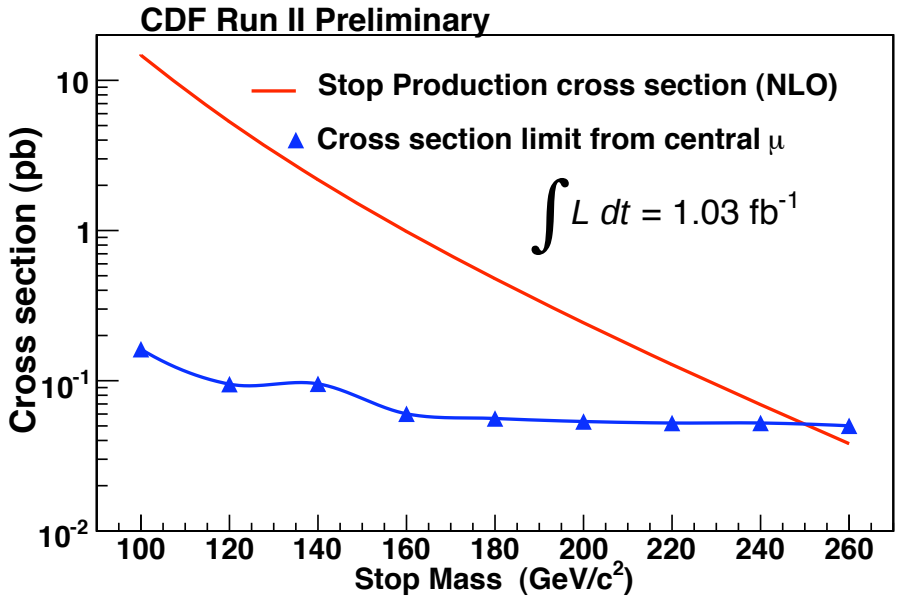

Figure 40: The theoretical NLO cross section for stop production, calculated using the Prospino program [22], is plotted as a function of stop mass (red), along with the cross section limit for the observed CMUP result and the efficiencies shown in Table 5.

data. We show that the resulting background from time mis-measurements — a contribution that would otherwise limit the sensitivity of the analysis — is both predictable and small.

In a model-independent search for slowly-moving, high-$p_{\rm t}$ particles, we observe no events with a reconstructed TOF mass above 100 GeV/c^2. The expected background above 100 GeV/c^2 is 2.1 events. Interpreting this result within the context of a model with a stable stop squark, we exclude at 95% C.L. masses of a stable stop between 100 GeV/c^2 and 250 GeV/c^2.

11 Appendix: Changes between Blessing and Re-blessing

Between the blessing and the reblessing we changed the prior used in determining the limits. For the blessing, we used the Bayesian statistics program bayesian-limit.tar.gz provided by the CDF statistics committee [23] with $\alpha = 0.5$, which corresponds to a prior of $1/\sqrt{s}$ where s is the signal. We chose this prior because it is listed as a "typical" choice in the Users Guide [24] and we have prior knowledge about the signal from earlier measurements (an upper limit). While this choice is defensible, the other "typical" choice of $\alpha = 1$ (a flat prior) is conventionally used for setting limits. We have therefore changed the limit calculation to use a flat prior.

We have also increased the Monte Carlo statistics for the lower-mass points. The limited statistics available at the time of the blessing substantially increased the uncertainty on the acceptance estimates for these points, which artificially affected the shape of the limit curve. We have also improved the error analysis in the total efficiency calculation, which now better accounts for common errors. The efficiencies have been re-organized in the process to separate event efficiencies from track-level efficiencies. This note has been updated to reflect this new organization.

The lowest stop mass we consider has been extended from 120 GeV/c^2 to 100 GeV/c^2 in order to overlap with previously published CHAMP limits. When we do this, we start to pick up some (presumed) background events in the window used for event counting at the lowest masses probed.

We have also produced the next generation (v14a) of our ntuple ChampNt. This is significant because the previous version (v13) of the ntuple did not apply TOF quality cuts to t_0 tracks when calculating the COT χ^2 for TOF β. This cost a considerable amount of acceptance since we cut on this χ^2, so we excluded events where this t_0 did not match the t_0 obtained when the TOF quality cuts are applied. Our acceptance has been significantly improved with this limitation removed. The new ntuple gives us the ability to further increase our acceptance, but for the purposes of reblessing we have attempted to keep the analysis the same as the blessed analysis. We are to implement the improvements for the expanded dataset.

Finally, we are now using the Prospino2 program [22] to calculate the NLO theoretical cross section. The previous result was based upon the Pythia cross section, which is only leading order.

References

[1] M. Drees and X. Tata, Physics Letter B **252** 695 (1990).

[2] R. Barbieri, L.J. Hall, Y. Nomura, **Phys Rev D** 63, 105007 (2001).

[3] J.L. Feng and T. Moroi, *Tevatron Signatures of Long-lived Charged Sleptons in Gauge-Mediated Supersymmetry Breaking Models*, hep-ph/9712499 (Dec. 1997).

[4] P.H. Frampton and P.Q. Hung, *Long-lived Quarks?*, hep-ph/9711218 (Nov. 1997).

[5] See for example: Lisa Randall and Raman Sundrum, *Out of This World Supersymmetry Breaking*, hep-th/9810155 (Apr. 1999);
H. Baer, K. Cheung, and J.F. Gunion, *A Heavy Gluino as the Lightest Supersymmetric Particle* hep-ph/9806361, (Sept. 1998);

[6] P.F. Smith *et al.*, Nucl. Phys. **B206**, 333 (1982); Byrne, Kolda and Regan, Phys. Rev. **D66**, 075007 (2002)

[7] CDF Collaboration, Phys. Rev. Lett. **90**, 131801 (2003).

[8] ALEPH Collaboration, Phys Lett **B537**, 5 (2002).

[9] LEP2 SUSY Working Group, LEPSUSYWG/02-05.1 (2002).

[10] W. Orejudos and F.D. Snider, *Run 2 CHAMP search*, CDF Note 6307.

[11] The D0 Collaboration, D0 public note.

[12] See http://www-cdf.fnal.gov/internal/dqm/goodrun/v13/goodv13.html.

[13] L. Nodulman, *Curvature corrections for 5.3.1 and 6.1.1*, CDF Note 6971.

[14] H.K. Gerberich, A.V. Kotwal, C. Hays, *Cosmic Ray Tagging using COT Hit Timing*, CDF Note 6089.

[15] K. Anikeev, *et al.*, *Construction and Installation of the CDF Time-of-Flight Counters for Run II*, CDF Note 5818.

[16] J. Beringer, *et al.*, The Time-of-Flight Reconstruction, CDF Note 7581.

[17] F.D. Snider, talk presented to the Feb. 17, 2006 B-Physics Analysis Kernel group (pdf).

[18] Thomas J. Phillips, *Event t0 from the COT and CLC*, CDF Note 6277.

[19] Monica D'Onofrio, *et al.*, talk presented to the Sept. 3, 2004, Joint Physics meeting (pdf).

[20] U. Grundler, A. Taffard, X. Zhang *High-P_T muons recommended cuts and efficiencies for Summer 2006*, CDF Note 8262.

[21] U. Grundler, L. Lovas, A. Taffard *High-P_T muons recommended cuts and efficiencies for Winter 2007*, CDF Note 8618.

[22] http://people.web.psi.ch/spira/prospino/manual.ps.gz

[23] http://www-cdf.fnal.gov/physics/statistics/statistics_software.html

[24] Joel Heinrich for the CDF Statistics Committee, *User Guide to Bayesian-Limit Software Package*, CDF Note 7232.